06

Aluminothermic synthesis of MnSi and $MnSi_{1.73}$: thermoelectric and magnetic properties

© A.E. Sytschev, S.L. Silyakov, A.O. Sivakova, Yu.G. Morozov, A.V. Karpov

Institute of Structural Macrokinetics and Materials Science Problems, Russian Academy of Sciences, Chernogolovka, Russia
E-mail: sivakovaalina@yandex.ru

Received June 9, 2025
Revised September 8, 2025
Accepted September 15, 2025

The paper presents the results of an investigation into the synthesis of manganese silicides MnSi and $MnSi_{1.73}$, which was performed using the aluminothermic reduction of metal oxides. Thermoelectric and magnetic properties of the obtained compounds have been studied. X-ray phase analysis showed that the alloy synthesized from reaction mixture (MnO_2+Si+Al) is a single-phase compound with monosilicide silicon detected in its composition. However, the alloy synthesized from reaction mixture (MnO2+Si+Al) is not single-phase as it contains phases such as $MnSi_{1.735}$, $Mn_2Al_5Si_5$ and a small amount of unreacted silicon. The alloys' microstructure consists in a homogeneous matrix with uniformly distributed pores. Thermoelectric measurements have revealed that the sample prepared from mixture MnO_2+Si+Al exhibits hole conductivity, Seebeck coefficient of $S = 30\,\mu$V/K at 400 K, and electrical resistance of $\rho = 290\,\mu\Omega \cdot$ cm cm at 1050 K. It was also shown that the alloys exhibit for MnSi (a) a distinct ferromagnetic behavior with saturation magnetization σ_s corresponding to $\sim 0.5\,\mu$B (Bohr magneton) per Mn atom.

Keywords: Seebeck coefficient, thermoelectric alloy, magnetic properties, aluminothermal synthesis.

DOI: 10.61011/TPL.2026.01.62825.20400

Intermetallic compounds based on manganese silicides Mn−Si are attractive for research in the field of magnetism aimed at developing new rare-earth-free permanent magnets and magnetic materials with good spin-electronic properties [1]. The Mn elementary magnetic moment is higher than that of Fe and Co, and Mn atoms are prone to antiferromagnetic interactions which reduce the total magnetization and Curie temperature ($T_c \approx 590$ K) [2]. Studies of thermoelectric properties of the manganese silicide phases have shown that the best characteristics are exhibited by those of higher manganese silicide $MnSi_{1.73}$. Manganese silicides $MnSi_x$ with $x = 1.71-1.75$ (typically denoted as $MnSi_{1.73}$) have attracted increased attention in view of developing optoelectronic and thermoelectric materials [3]. Phases of higher manganese silicide $MnSi_{1.73}$ and manganese monosilicide MnSi exist in a narrow range of manganese concentrations in silicon and may coexist in thermodynamic equilibrium due to an enlarged region of the Mn−Si phase diagram. The Si solubility in β-Mn at 1060 °C is 16.7 at.%, that in α-Mn at $\sim$ 635 °C is 6.0 at.%; the solubility decreases with increasing temperature. Mn is almost fully insoluble in Si [4]. The process dominating during the formation of phases MnSi and $MnSi_{1.73}$ is silicon diffusion [5]. The high-temperature reaction first of all leads to formation of MnSi (melting point of 1060−1285 °C, density of 6.1 g/cm^3). Further, along with enrichment with silicon, phase $MnSi_{1.73}$ is being formed.

In [6], compound $MnSi_{1.73}$ was obtained by spark plasma sintering. Self-propagating high-temperature synthesis is one of the methods for obtaining refractory compounds such as borides, nitrides, carbides, as well as silicides [7] of transition metals Mo, Ti, Zr, Nb and Ta. Synthesis of transition-metal silicides may also be performed in the combustion mode based on the aluminothermic reduction of metal oxides [8]. Specific features of the synthesis (directly in the process of sintering) of higher manganese silicide from nanopowders in a setup for electric-pulse plasma sintering were considered in [6].

In this work, MnSi and $MnSi_{1.73}$ were obtained by the method of aluminothermic reduction of manganese (IV) oxide. As components of the initial thermite-type exothermic mixtures, powders of approximately equal dispersion were used: manganese (IV) oxides (particle size $d_{50} = 34\,\mu$m), „Pure“ silicon oxide (particle size $d_{50} = 36\,\mu$m), aluminum ASD-1 (particle size $d_{50} = 33\,\mu$m) and silicon KR-0 (particle size $d_{50} = 7\,\mu$m). Reaction mixtures of the powders were prepared in the proportions indicated in Table 1. Prior to mixing, the initial powders were dried for 3 h. These exothermic thermite-type mixtures were selected so as to produce manganese silicides based on silicon and silicon oxide through the following chemical reactions, respectively:

$$\gamma_1 MnO_2 + \gamma_2 Si + \gamma_3 Al \rightarrow \gamma_4 MnSi_x + \gamma_5 Al_2O_3, \qquad (1)$$

Table 1. Compositions of reaction mixtures and rated adiabatic combustion temperatures T_{ad}

Reaction mixture composition, mass %				T_{ad}, K
MnO_2	Al	Si	SiO_2	
62.9	11.0	26.1	–	3150
49.7	31.7	–	18.6	3080

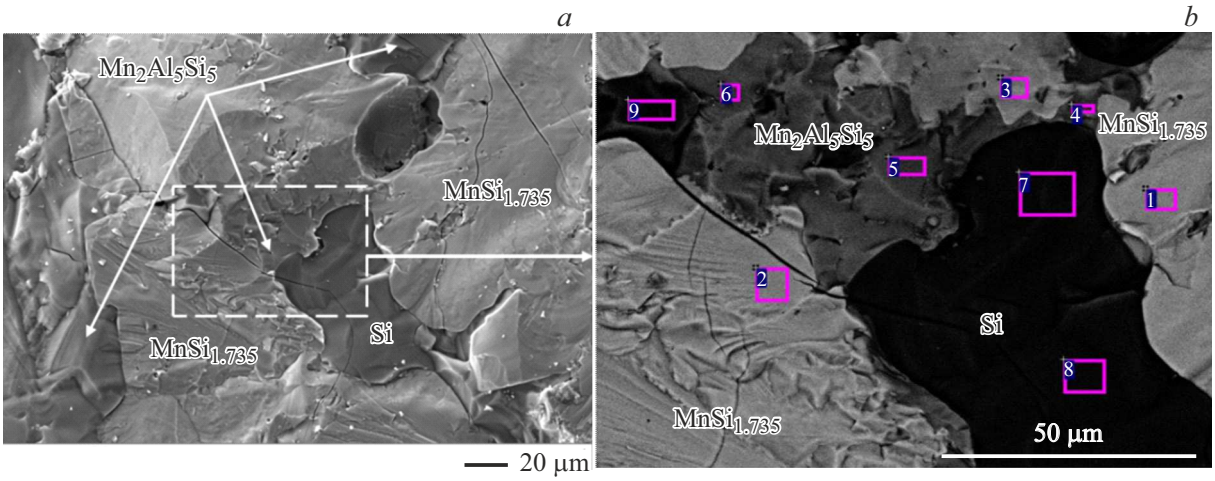

Figure 1. SEM microimages of the sample combustion products. *a* — general view, *b* — scaled-up fragment (indicated with the dashed line in panel *a*) of reaction mixture MnO_2+SiO_2+Al; numbered rectangles indicate the regions where EDA spectra were measured.

$$\gamma_6 MnO_2 + \gamma_7 SiO_2 + \gamma_8 Al \rightarrow \gamma_9 MnSi_x + \gamma_{10} Al_2O_3, \quad (2)$$

where $\gamma_1-\gamma_{10}$ are the stoichiometric coefficients, x is the silicon percentage in manganese silicide.

Manganese silicides were synthesized from exothermic thermite-type mixtures 100 g in mass in a reactor 31 in volume, 40 mm in internal diameter and 70 mm in height at the bulk density of 0.87g/cm^3 in argon with the initial pressure of 5 MPa. Ignition was performed by using a tungsten coil. Preliminary thermodynamic calculations of the adiabatic combustion temperatures for the exothermic compositions under study via program code „Thermo“ [9] are presented in Table 1.

After the combustion front passed through the reaction mixture, the combustion products remained in the liquid state in the form of a melt which, being cooled, was photo-separated into the „oxide“ (ceramic) and „metallic“ layers. Characteristic dimensions of the metallic layer were as follows: diameter of 30 mm, thickness of 15 mm. Upon cooling, the samples were removed from the reactor, and the „metallic“ layer was mechanically separated for further study. Phase compositions of the combustion products were analyzed using computer-aided X-ray diffractometer DRON-3M (FeK_α radiation). The synthesized alloy microstructures were studied with a Zeiss Ultra plus ultra-high-resolution scanning electron microscope (SEM) based on Ultra 55 with microanalysis system INCA Energy 350 XT (Oxford Instruments). Temperature dependence of electrical resistivity was measured in vacuum of 10^{-5} mm Hg in the temperature range of 300−1100 K by using the standard DC four-point method. ThermoEMF was obtained using a laboratory setup for measuring the Seebeck coefficient in the temperature range of 300−800 K. Magnetic characteristics of the synthesized samples were determined using vibrating magnetometer EG&G PAR M4500 in magnetic fields up to 10 kOe.

The alloy synthesized from mixture MnO_2+Si+Al (Table 1) is single-phase and consists in the cubic-syngony manganese monosilicide MnSi (PDF 65-5372) (space group $P2_13$); its microstructure has the form of a dense matrix with uniformly distributed spherical pores up to 50 μm in diameter. Pores get formed due to reduction reaction (1) accompanied by release of the gaseous products, namely, aluminum oxide (I) Al_2O and Al. Data of energy dispersive analysis (EDA) correlate with the results of X-ray phase analysis and confirm formation of manganese monosilicide MnSi.

Phase composition of the product synthesized from reaction mixture MnO_2+SiO_2+Al (Table 1) is as follows: the main tetragonal-syngony phase $MnSi_{1.735}$ (PDF 01-0412), tetragonal-syngony solid solution $Mn_2Al_5Si_5$ (PDF 54-0360), and insignificant amount of cubic-syngony Si (PDF 27-1402) (space group Fd_3m) (Fig. 1). Intensity of peaks corresponding to the $Mn_2Al_5Si_5$ phase is low, which evidences for low concentration of this phase in the sample under study. The MnSi structure is the α derivative and crystallizes in the cubic space group $P2_13$ [10]. The presence of a small amount of Si indicates incompleteness of the oxides MnO_2 and SiO_2 reduction ((see (2)) in the initial reaction mixture. Microstructure of the sample synthesized from reaction mixture MnO_2+SiO_2+Al also is a dense matrix with spherical pores up to 50 μm in size uniformly distributed throughout the volume. EDA data show the presence of 10.7 at.% of Al included in solid solution $Mn_2Al_5Si_5$. Fig. 1 demonstrates with high resolution a fragment of the sample microstructure where all three phases are indicated: $MnSi_{1.735}$, $Mn_2Al_5Si_5$ and Si; this complies with the X-ray phase analysis data. The reduced silicon exists in the intergranular space of $MnSi_{1.735}$, $Mn_2Al_5Si_5$ in the form of individual inclusions up to 100 μm in size.

Fig. 2 presents the temperature dependence of electrical resistivity ρ for the synthesized alloy in the heating-cooling mode. Electrical resistivity was measured in the temperature range of 300 to 1100 K. The room-temperature resistivity

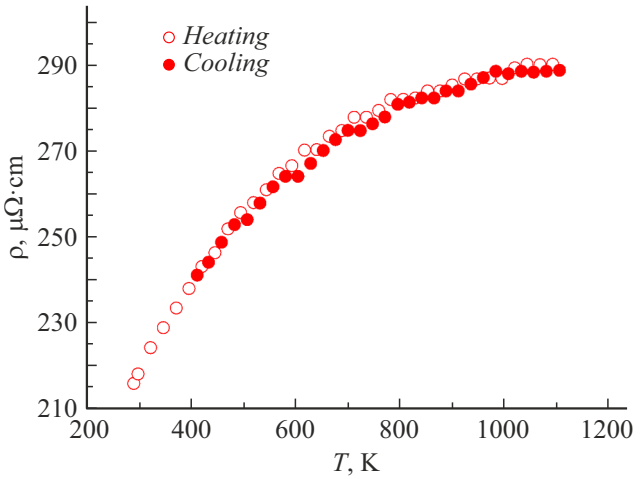

Figure 2. Electrical resistivity of the MnO_2+Si+Al alloy versus temperature in the heating-cooling cycle.

is $215\,\mu\Omega\cdot$cm. Over the entire temperature range under consideration, the resistivity increases monotonically and reaches its highest value $290\,\mu\Omega\cdot$cm at the maximum temperature of 1100 K. It is important to emphasize that the results repeat in multiple heating-cooling thermal cycles, which indicates the absence of phase transformations and variations in the material structure within this temperature range, and also confirms stability of the sample's crystalline structure.

Fig. 3 presents the temperature dependence of thermoelectromotive force (thermoEMF) for the synthesized alloy in the temperature range of 300−800 K. The Seebeck coefficient dependence is nonlinear and is represented by a curve with the maximum at 400 K. Room-temperature S is about $28\,\mu$V/K; then maximum $S = 30\,\mu$V/K is observed at $T = 400$ K after which S uniformly decreases to $23\,\mu$V/K at 800 K. This factor remains positive over the entire temperature range under study, which proves the predominance of

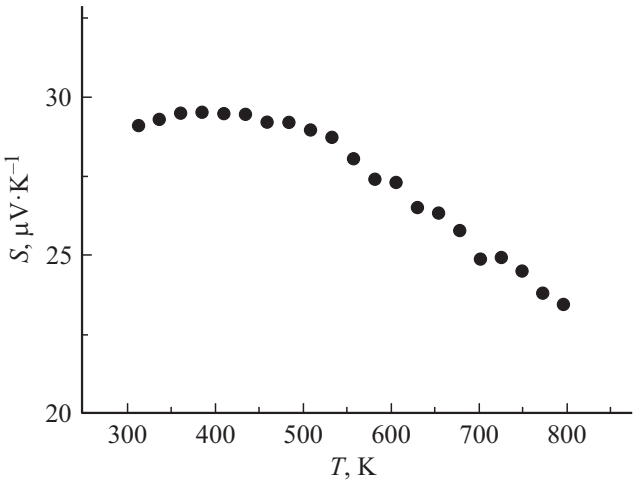

Figure 3. Seebeck coefficient of synthesized alloy MnO_2+Si+Al versus temperature.

the hole-type conductivity of the alloy. Most likely, the type of dependencies $S(T)$ is determined by the thermoEMF diffusion component and is caused by specific features of the band structure, as well as by the processes of charge carrier scattering inherent to semi-metallic ferromagnets studied in [11] where a similar dependence was observed.

Fig. 4 presents magnetization curves of the samples synthesized from reaction mixtures MnO_2+Si+Al and MnO_2+SiO_2+Al at room temperature. Based on the data of Table 2, it is possible to estimate that saturation magnetization σ_s of the MnSi alloy (Fig. 4, *a*) matches value $\sim 0.5\,\mu_B$ (Bohr magneton) per Mn atom. This shows [12] that nearly 10 % of the Mn atoms participate in the exchange coupling if each Mn atom has an isolated Mn-atom magnetic moment of $5\mu_B$. MnSi possesses a very complex magnetic phase diagram containing, along with regions of helicoid ferromagnetic spirals and magnetic-field-induced ferromagnetism, phases of skyrmion lattices and fluctuations of these spirals [13], whereat the temperature of the ferromagnet−paramagnet magnetic phase transition at the atmospheric pressure is about 29 K [14].

For the MnO_2+SiO_2+Al alloy, it is possible to assume that in this case high-temperature ferromagnetism is explained by formation of defects with local magnetic moments [14] and also by their indirect exchange through paramagnetic fluctuations of the hole spin density [15]. In addition, there may take place separation of the material phases, when Mn atoms are collected in nanoparticles consisting of $MnSi_{2-z}$ with $z \approx 0.25-0.30$, which are embedded in the silicon matrix with low content of Mn. Such a material may contain a certain number of magnetic defects arising due to unbound Mn 3*d*-orbitals and be a weak band ferromagnet in which significant spin fluctuations exist well above its intrinsic Curie temperature, which leads to a significant enhancement of exchange coupling between local defect moments and increase in the temperature of occurrence of the long-range order among those moments [16].

Thus, in this study single-phase manganese monosilicide MnSi and alloy containing the tetragonal-syngony main phase $MnSi_{1.735}$ (PDF 01-0412), tetragonal-syngony solid solution $Mn_2Al_5Si_5$ (PDF 54-0360) and insignificant amount of cubic-syngony Si (PDF 27-1402) (space group Fd_3m) were synthesized for the first time by the method of aluminothermic reduction of manganese (IV) oxide with aluminum. The fact that the Seebeck coefficient remains positive over the entire interval evidences that charge carriers in this material are holes. Alloy MnO_2+Si+Al exhibits obvious ferromagnetic properties matching the value of $\sim 0.5\,\mu_B$ per Mn atom. However, alloy MnO_2+SiO_2+Al exhibits high-temperature ferromagnetism associated with formation of defects with local magnetic moments.

Funding

The study was performed under the State Assignment to ISMAN.

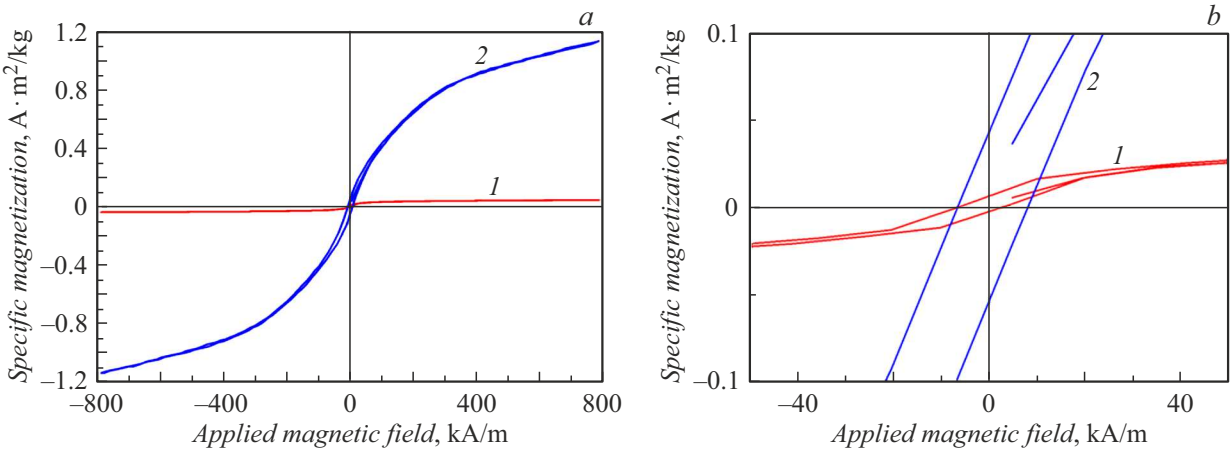

Figure 4. *a* — magnetization curves of samples synthesized at room temperature from reaction mixtures MnO_2+Si+Al (*1*) and MnO_2+SiO_2+Al (*2*). *b* — scaled-up fragments.

Table 2. Saturation magnetization σ_s, residual magnetization σ_r and coercivity H_c of the synthesized alloys

Initial composition	σ_s, A · m²/kg	σ_r, A · m²/kg	H_c, kA/m
MnO_2+Si+Al	0.042	0.0046	4.77
MnO_2+SiO_2+Al	1.13	0.048	7.40

Conflict of interests

The authors declare that they have no conflict of interests.

References

[1] A.M. Tishin, Y.I. Spichkin, *The magnetocaloric effect and its applications* (CRC Press, Boca Raton, 2003). DOI: 10.1201/9781420033373
[2] C.-H. Lee, H.-H. Chin, K.-Y. Zeng, Y.-J. Chang, A.-C. Yeh, J.-W. Yeh, S.-J. Lin, C.-C. Wang, U. Glatzel, E.-W. Huang, Front. Mater., **9**, 824285 (2022). DOI: 10.3389/fmats.2022.824285
[3] Z. Wang, Y. Wu, Y. He, Int. J. Mod. Phys. B., **18** (1), 87 (2004). DOI: 10.1142/S0217979204023702
[4] *Diagrammy sostoyaniya dvoynykh metallicheskikh system: spravochnik*, pod obshch. red. N.P. Lyakisheva (Mashinostroenie, M., 1996), t. 1–3. (in Russian)
[5] L. Zhang, D.G. Ivey, Int. J. Mater. Res., **6**, 1518 (1991). DOI: 10.1557/JMR.1991.1518
[6] A.R. Sarkisyan, S.K. Dolukhanyan, I.P. Borovinskaya, Powder Metall. Met. Ceram., **17**, 424 (1978). DOI: 10.1007/BF00795793
[7] V.A. Gorshkov, P.A. Miloserdov, D.D. Titov, V.I. Yukhvid, Yu.F. Kargin, Inorg. Mater. Appl. Res., **10**, 473 (2019). DOI: 10.1134/S2075113319020138
[8] Yu.M. Kuznetsov, M.V. Dorokhin, I.L. Kalentyeva, A.V. Zdoroveyshchev, P.B. Demina, I.V. Erofeeva, V.N. Trushin, M.S. Boldin, E.A. Lancev, Semiconductors, **58** (7), 345 (2024). DOI: 10.61011/SC.2024.07.59543.6350H.
[9] *Program for thermodynamics equilibrium calculations „THERMO“* [Electronic source]. https://ism.ac.ru/thermo/
[10] https://next-gen.materialsproject.org/materials/mp-1431?chemsys =Mn-Si#how_to_cite
[11] N.I. Kourov, V.V. Marchenkov, A.V. Korolev, L.A. Stashkova, S.M. Emel'yanova, H.W. Weber, Phys. Solid State, **57** (4), 700 (2015). DOI: 10.1134/S1063783415040149.
[12] M. Bolduc, C. Awo-Affouda, A. Stollenwerk, M.B. Huang, F.G. Ramos, G. Agnello, V.P. LaBella, Phys. Rev. B, **71**, 033302 (2005). DOI: 10.1103/PhysRevB.71.033302
[13] A.A. Povzner, A.G. Volkov, M.A. Chernikova, Phys. Solid State, **65** (12), 2151 (2023). DOI: 10.61011/PSS.2023.12.57688.189.
[14] O.V. Belousova, I.D. Kovalev, A.E. Sytschev, Eurasian Chem.-Technol. J., **21** (4), 347 (2019). DOI: 10.18321/ectj892
[15] V.V. Rylkov, S.N. Nikolaev, K.Yu. Chernoglazov, B.A. Aronzon, K.I. Maslakov, V.V. Tugushev, E.T. Kulatov, I.A. Likhachev, E.M. Pashaev, A.S. Semisalova, N.S. Perov, A.B. Granovskii, E.A. Gan'shina, O.A. Novodvorskii, O.D. Khramova, E.V. Khaidukov, V.Ya. Panchenko, JETP Lett., **96**, 255 (2012). DOI: 10.1134/S0021364012160114.
[16] V.N. Men'shov, V.V. Tugushev, S. Caprara, E.V. Chulkov, Phys. Rev. B, **83**, 035201 (2011). DOI: 10.1103/PhysRevB.83.035201

Translated by EgoTranslating